# Universal transparency and asymmetric spin splitting near the Dirac point in HgTe quantum wells

V. Dziom,[1,*] A. Shuvaev,[2] J. Gospodarič,[2] E. G. Novik,[3] A. A. Dobretsova,[4,5] N. N. Mikhailov,[4,5] Z. D. Kvon,[4,5] Z. Alpichshev,[1] and A. Pimenov[2]

[1]*Institute of Science and Technology Austria, 3400 Klosterneuburg, Austria*
[2]*Institute of Solid State Physics, Vienna University of Technology, 1040 Vienna, Austria*
[3]*Institute of Theoretical Physics, Technische Universität Dresden, 01062 Dresden, Germany*
[4]*Rzhanov Institute of Semiconductor Physics, 630090 Novosibirsk, Russia*
[5]*Novosibirsk State University, 630090 Novosibirsk, Russia*

(Received 9 February 2022; accepted 17 June 2022; published 11 July 2022)

Spin-orbit coupling in thin HgTe quantum wells results in a relativistic-like electron band structure, making it a versatile solid state platform to observe and control nontrivial electrodynamic phenomena. Here we report an observation of universal terahertz (THz) transparency determined by fine-structure constant $\alpha \approx 1/137$ in 6.5-nm-thick HgTe layer, close to the critical thickness separating phases with topologically different electronic band structure. Using THz spectroscopy in a magnetic field we obtain direct evidence of asymmetric spin splitting of the Dirac cone. This particle-hole asymmetry facilitates optical control of edge spin currents in the quantum wells.

DOI: 10.1103/PhysRevB.106.045302

## I. INTRODUCTION

While advance in fundamental high-energy physics requires increasingly larger and more expensive facilities, solid crystals provide an alternative platform allowing exploration of relativistic electrodynamics. Interaction of an electron with the crystal field leads to a modification of the energy vs momentum relation. In particular cases it results in a relativistic-like dispersion, the most well-known example being graphene. The relativistic spectrum leads to various unusual electrodynamic phenomena [1–13]. The highest-quality graphene is currently available in the form of microscopic flakes, and great efforts are being made to improve techniques for production of macroscopic sheets. Demand for larger defect-free samples is coming not only from practical applications, but also from fundamental research, because usage of numerous powerful experimental methods is impossible or strongly limited for microscopic samples.

Two-dimensional electronic states with relativistic-like spectrum can also be realized in HgTe/CdHgTe heterostructures, grown using molecular beam epitaxy (MBE). Constant improvement in the technology of growth [14] and creation of semitransparent gates made it possible to use magneto-optical terahertz (THz) spectroscopy to study fine details of the electronic spectrum around the Dirac point. In present work we report the observation of universal transmission of coin-sized HgTe/CdHgTe heterostructures defined by the fundamental quantum fine-structure constant $\alpha = e^2/(4\pi\varepsilon_0\hbar c) \approx 1/137$. Unlike the optical quantum Hall effect (QHE) [6,7,15,16] and similar to the anomalous QHE [17], in the reported case the universal absorption $\pi\alpha/2 \approx 1.1\%$ is observed in zero magnetic field, while the application of a magnetic field only facilitates the measurement of this tiny effect. Also, our study of the cyclotron resonance provides direct evidence of significant electron-hole asymmetry at the Dirac point, that we attribute to much stronger spin splitting in the valence band. Using the semiclassical approach we reconstruct fine details of the band structure around the Dirac point. The particle-hole asymmetry, that can be useful in quantum devices like nanotransistors [18] and magnetically tunable lasers [9], has been long overlooked in theoretical models for CdHgTe heterostructures. Recent theoretical works [19–23] suggest that particle-hole asymmetries of bulk states enable photoinduced spin-polarized DC currents in the helical edge states of CdHgTe quantum wells.

## II. THEORY: BAND STRUCTURE AND INTERBAND ABSORPTION

Electronic band structure in the family of cadmium-mercury telluride ($HgTe/Cd_{1-x}Hg_xTe$) quantum wells can be engineered by a growth procedure [24–26]. The energy gap strongly depends on the thickness $d$ of the HgTe layer and weakly on the barrier composition $x$. HgTe wells with thickness around $d_c = 6.5$ nm demonstrate a vanishing gap in transport measurements. Interest in these quantum wells was greatly enhanced when the calculation of the band structure using the $\mathbf{k}\cdot\mathbf{p}$ model [24] predicted a topological transition with the relativistic electron spectrum

$$E(\mathbf{k}) = \pm\sqrt{\delta^2 + (v_F\hbar\mathbf{k})^2}, \quad (1)$$

*udziom@ist.ac.at

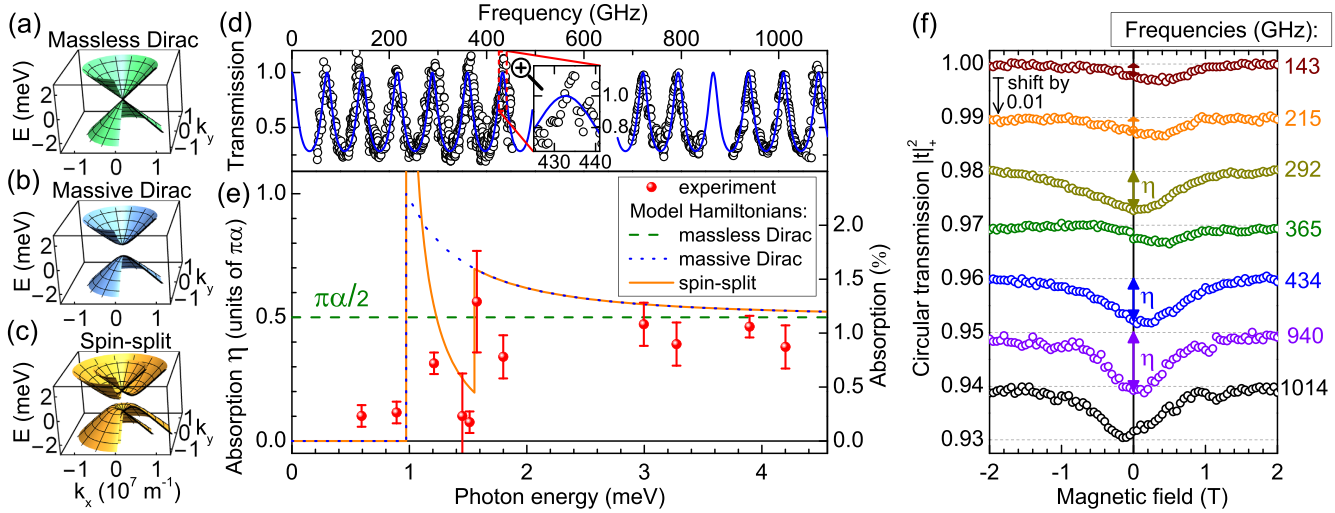


FIG. 1. Observation of absorption defined by the fine-structure constant $\alpha$ in macroscopic HgTe/CdHgTe heterostructures. (a)–(c) Electronic band structure in several theoretical models. (d) Directly measured transmission coefficient for THz radiation in zero field at 1.85 K. (e) Absorption in zero field as extracted from field dependence of transmission at fixed frequencies (f).

where the band gap $2|\delta| \propto |d_c - d|$ in the vicinity of $d_c$ and turns to zero at $d = d_c$. In this simple model at $d = d_c$ the bands form an axial-symmetric spin-degenerate cone shown in Fig. 1(a), corresponding to a massless relativistic Dirac quasiparticle. If the Fermi level is tuned to the Dirac point, e.g., the lower half of the cone is filled, and a plane electromagnetic wave passes through the two-dimensional (2D) system, the electric field will induce vertical electron transitions between the valence and conduction bands, leading to energy absorption rate $\pi\alpha/2 \approx 1.1\%$, shown in Fig. 1(e) by the green dashed line. The value of absorption does not depend on the material parameter $v_F$ in a range of photon energies, thus demonstrating so-called universal behavior. In graphene [25,27] the twofold valley degeneracy leads to the twice higher absorption equal to $\pi\alpha$. Energy independence of the absorption allows a simple intuitive explanation based on dimensional analysis [28]: the linear spectrum $E = v_F\hbar k$ does not contain any energy scales to form a dimensionless combination with the photon energy for dimensionless absorption $\eta(\hbar\omega)$.

A realistic HgTe quantum well consists of an integer number of atomic layers, and its thickness cannot exactly match the theoretical value. Samples with nominally critical thickness can demonstrate small band gaps of the order of several meV. Opening of the gap in spectrum (1) leads to modification of absorption [24,27,29] at photon energies $\hbar\omega \lesssim 2|\delta|$ as shown in Fig. 1(e) by the blue dotted line. The quantum well does not absorb radiation with the photon energy $\hbar\omega < 2|\delta|$, and just above the band gap the absorption is doubled. At photon energies much higher than the gap $\hbar\omega \gg 2|\delta|$ absorption tends to the gap-independent value $\eta_0 = \pi\alpha/2$.

Derivation of the seminal model [24] for the Dirac spectrum (1) used simplifications that led to spin-degenerate solutions for electron states. Later the model was modified [29–33] to allow for the bulk inversion asymmetry of host CdHgTe and HgTe crystals and the inversion asymmetry of their interface. In Ref. [29] the modified effective Hamiltonian has a solution in the form of spin-split electron-hole symmetric bands

$$E(\mathbf{k}) = \mp\sqrt{\delta^2 + (v_F\hbar k \pm \gamma)^2}. \tag{2}$$

With parameters $\delta = \gamma = 0$ the model reproduces the linear massless cone in Fig. 1(a) and the frequency-independent absorption $\pi\alpha/2$. The small mismatch of the thickness to the critical value leads to nonzero $\delta$ [Fig. 1(b)]. Finally, parameter $\gamma$ effectively describes the spin splitting caused by inversion asymmetries of the crystals and the interfaces, shown in Fig. 1(c). Using equations in Ref. [29] we deduce expression for the real part of conductivity in an explicit form as

$$\sigma'_{xx}(E) = \frac{\pi\alpha}{Z_0} \times \begin{cases} 0 & \text{if } |E| \leqslant 2|\delta|, \\ \frac{4|\gamma|\delta^2}{E^2\sqrt{E^2-4\delta^2}} & \text{if } 2|\delta| < |E| < 2\sqrt{\delta^2+\gamma^2}, \\ \frac{1}{2} + \frac{2\delta^2}{E^2} & \text{if } |E| \geqslant 2\sqrt{\delta^2+\gamma^2}, \end{cases} \tag{3}$$

where $E = \hbar\omega$ is the photon energy and $Z_0$ is the vacuum impedance. An example of absorption $\eta = Z_0\sigma'_{xx}$ calculated within this model is shown as the solid orange line in Fig. 1(e) for parameters $2\delta = 0.97$ meV and $2\gamma = 1.21$ meV giving the optimal fit to the experimentally determined absorption in a 6.5 nm HgTe quantum well. The theoretical curve has an absorption peak at $\hbar\omega = 2|\delta|$ and a local minimum in absorption just below $\hbar\omega = 2\sqrt{\delta^2+\gamma^2}$. At high energies $\hbar\omega \gg 2\sqrt{\delta^2+\gamma^2}$ absorption asymptotically tends to $\pi\alpha/2$.

## III. EXPERIMENTAL TECHNIQUES AND DATA TREATMENT

### A. Samples

CdHgTe quantum wells with well thicknesses of 6.5 and 7.1 nm were grown by molecular beam epitaxy on (013)-oriented GaAs substrates [26,34–36]. A 5-$\mu$m-thick initial buffer layer was grown first. The HgTe quantum well is stacked between two 30-nm-thick $Cd_{0.65}Hg_{0.35}Te$ layers to increase the charge carriers' mobility. Symmetrical doping with indium was introduced between buffer and capping layers to

TABLE I. HgTe/CdHgTe quantum wells used in the experiments. Here $d$ is the nominal thickness of the HgTe well and $n$ is the total density of charge carriers at 1.85 K in a sample cooled in darkness.

| Sample # | $d$ (nm) | Wafer ID | $n$ (cm$^{-2}$) | Dimensions (mm$^3$) |
|---|---|---|---|---|
| 1 | 6.5 | 170315 | $5.0 \times 10^{10}$ (hole, from DC) | $10 \times 10 \times 0.600$ |
| 2 | 6.5 | 170315 | $2.2 \times 10^{10}$ (hole, from THz) | $10 \times 10 \times 0.600$ |
| 3 | 7.1 | 110624 | $1.5 \times 10^{10}$ (hole, from THz) | $10 \times 10 \times 0.394$ |

put the Fermi level close to the charge neutrality point. The samples allowed using 10 mm aperture and also had four Ohmic contacts at the corners to allow *in situ* transport measurements in van der Pauw geometry. Control of the charge carriers' density was achieved through light illumination using the effect of persistent photoconductivity [26,37,38].

The samples studied in this work are listed in Table (I). Samples #1 and #2 were cut from the same wafer with nominal HgTe thickness 6.5 nm. For equal doping levels samples #1 and #2 produced identical data, showing that the wafer was highly uniform. They differed only by the initial charge density, which is also dependent on the prehistory. In particular, the initial Fermi level in a dark-cooled sample can change randomly after remounting in the cryostat.

Sample #3 was cut from another wafer with nominal HgTe thickness 7.1 nm. Similarly to samples #1 and #2, sample #3 also demonstrated clear spin splitting in the valence band. Control of the Fermi level by illumination was limited by a much smaller range of available densities and we could not reach the charge neutrality point: even in the room light the sample #3 still demonstrated hole response. The smaller range of densities may be a consequence of a cleaner GaAs substrate, as the defects in the substrate serve as the source of electrons in the effect of persistent photoconductivity.

### B. Spectrometer

Absorption of THz light in CdHgTe wells was determined using a continuous wave spectrometer. Backward wave oscillators (BWO) served as a source of continuous linearly polarized monochromatic radiation. Intensity of radiation was measured by a 4 K He-cooled Si bolometer. Radiation beams were controlled in a quasioptical manner using Teflon lenses and metallic mirrors. The polarization of the beam was controlled by wire grid polarizers. The sample was immersed in pumped liquid helium ($T = 1.85$ K) inside an Oxford cryostat equipped with a superconducting 7 T magnet. The main measurement mode in the present work was to fix the frequency of the generated radiation and to measure the transmitted intensity of the circularly (subscript $\pm$) or linearly ($||$) polarized wave. The circular polarization was produced by an adjustable reflective retarder consisting of a wire grid and a flat mirror. In experiments we measure the absolute value of transmission coefficient determined as the ratio of intensities with and without the sample in the beam: $|t|^2 = I_s/I_0$.

### C. Fresnel equations: Getting conductivity from transmission coefficient

From the point of view of electrodynamics, a real heterostructure is represented by an infinitely thin conducting film (HgTe well) on a dielectric plane-parallel slab (GaAs substrate). Near the Dirac point, intraband semiclassical conductivity is suppressed, therefore absorption $\eta \ll 1$ in the well becomes small. First consider a free-standing well without a substrate. In this case reflection $|r|^2 \propto |\eta|^2$ is negligibly small, while transmission $|t|^2$ and absorption $\eta$ are determined by the real part of complex dynamic conductivity $\sigma_{xx} = \sigma'_{xx} + \imath\sigma''_{xx}$:

$$\eta = Z_0\sigma'_{xx} = 1 - |t|^2, \tag{4}$$

where $Z_0 \approx 377\ \Omega$ is the impedance of free space. Therefore a sole measurement of $|t|^2$ is sufficient to determine absorption in the well and the real part of its conductivity.

In presence of a dielectric substrate, complex quantities $t$ and $\sigma_{xx}$ are related by an analytical equation that can be found in Ref. [39]. In order to determine $\sigma'_{xx}$ and $\eta$ at an arbitrary frequency, one generally needs to know the complex phase $\arg t$ as well. Although the measurement of the phase is technically possible using our Mach-Zehnder interferometer, the estimated phase shift due to the interband transitions is an order of magnitude smaller than experimental $\sim 1$ $\mu$m reproducibility. Fortunately, the corresponding Fresnel equations are greatly simplified in Fabry-Pérot transmission maxima, corresponding to the frequencies at which doubled substrate thickness equals an integer number of wavelengths in the dielectric. At these discrete frequencies the substrate effectively disappears from the equations and the sample behaves as a free-standing HgTe well, so that the phase is not needed to determine absorption and Eq. (4) is valid.

### D. Transmission coefficient: Removing effect of optical windows

Direct accurate measurements of transmission in an optical cryostat are complicated by reflections between the sample and the optical windows. Figure 1(d) shows experimentally determined transmission $|t|^2(\hbar\omega)$ (open symbols) through sample #1 as a function of frequency in zero field. This dependence is mainly governed by reflections at the surfaces of the GaAs substrate that lead to Fabry-Pérot oscillations with the period $c/(2a\sqrt{\varepsilon}) \approx 72$ GHz, where $c$ is the speed of light and $\varepsilon = 12$ is the dielectric permittivity of the GaAs substrate with thickness $a = 600$ $\mu$m. The bare substrate in free space would have transmission shown by the blue solid curve, calculated using an exact analytical equation [39]. Unaccounted reflections between the sample and the inner optical windows lead to the irregular (but reproducible) oscillatory deviation with a "period" around 5 GHz, which is better seen in inset in Fig. 1(d).

The problem was bypassed by measuring transmission at fixed frequencies as a function of applied magnetic field, as shown in Fig. 1(f). Within the accuracy limited mostly

by experimental reproducibility, transmission through the sample in the cryostat, $|t_w|$, is proportional to transmission through the sample in vacuum (no windows), $|t_v|$: $|t_w(\omega, B)| = \beta(\omega)|t_v(\omega, B)|$. The frequency-dependent coefficient $\beta$ is determined from the high-field transmission level: in the applied field $B_{high}$ of several tesla separation between Landau levels exceeds the photon energy and the well becomes fully transparent, $|t_v(\omega, B_{high})|^2 = 1$. Practically we divide the magnetic field dependence $|t_w(\omega, B)|^2$ by its high-field value to obtain transmission $|t|^2 = |t_v(\omega, 0)|^2$ in zero field and determine absorption using Eq. (4). Both circular and linear polarizations can be used for this purpose, because in zero field the transmission coefficients are equal: $t_{||}|_{B=0} = t_{\pm}|_{B=0}$.

## IV. RESULTS: UNIVERSAL ABSORPTION AND ASYMMETRIC SPIN SPLITTING

Experimental absorption is shown in Fig. 1(e) as a function of frequency (photon energy). For two points adjacent to 365 GHz that are out of a Fabry-Pérot maximum, absorption in HgTe well was recalculated using the complex phase from a spin-split model calculation, shown by the orange curve. At energies $\hbar\omega > 1.5$ meV experimental absorption tends to the universal value $\pi\alpha/2$, common for all the models discussed above. At low frequencies the well is almost transparent. The onset of significant absorption occurs at photon energies around 1 meV and we determine $E_g = 2\delta = 0.97$ meV from the spin-split model as an experimental estimate of the band gap to reconstruct the band structure, which is to be reported in a separate publication. The frequency dependence of absorption can be compared to the similar effect in graphene [27,28,40], where the universal value is twice higher because of two valleys. In graphene the low-energy absorbance is affected by unintentional doping, leading to the drop of absorbance at $\hbar\omega < 2E_F$ [28,41]. In HgTe wells the Fermi level can be precisely controlled by illumination with visible light, so that low energy absorption is determined by the small gap $E_g \simeq 1$ meV in the band structure. Another factor that may affect absorption dependence is the asymmetric spin splitting. Indirect evidence of a much stronger spin splitting in the valence band was demonstrated earlier in transport Shubnikov–de Haas (SdH) experiments in a tilted magnetic field [33]. Here we present a direct confirmation of the asymmetry revealed in magnetic field dependency of transmission at fixed frequencies. The most convenient way to demonstrate the effect is to fix the frequency and measure circular transmission as a function of magnetic field and the Fermi level. We show the data for 940 GHz on sample #1, since the splitting is more pronounced at high frequencies, and to provide another demonstration of the universal absorption at the Dirac point.

Figure 2(a) shows the circular transmission $|t_+|^2$ at 940 GHz as a function of perpendicular magnetic field and illumination time. In this experiment we sweep the magnetic field while the frequency and the Fermi level are fixed. Between the sweeps the Fermi level is tuned by the effect of persistent photoconductivity. Upon cooling down sample #1 in darkness we obtain the Fermi level in the valence band, with the density of holes $n_{Hall} = 5 \times 10^{10}\,\mathrm{cm}^{-2}$. This value, determined by intrinsic doping, was obtained by measuring $R_H$, the slope of the Hall resistance, shown in the inset in Fig. 2(b). By illuminating the sample with a green light-emitting diode we shifted the Fermi level by small steps through the charge neutrality point to the conduction band.

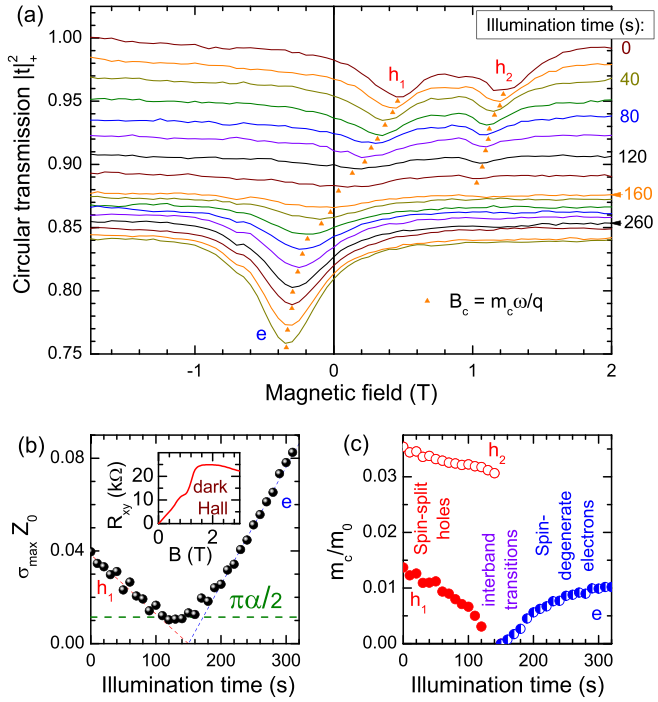


FIG. 2. Asymmetric spin splitting and universal absorption in transmission at fixed frequency. (a) Transmission of circularly polarized 940 GHz radiation at 1.85 K. The dark sample demonstrates two resonances at positive magnetic field, corresponding to spin-resolved hole subbands. Illumination shifts the Fermi level to the conduction band with much smaller spin splitting, and electrons produce the single resonance in the negative field. (b) Optical conductivity in resonances $h_1$ and $e$ takes the universal value $\pi\alpha/2$ upon passing through zero magnetic field. $Z_0$ is the vacuum impedance; dashed lines are guides to the eye. The inset shows *in situ* Hall resistance for the dark sample. (c) Cyclotron masses determined from positions of the resonances $e$, $h_1$, and $h_2$.

Each curve in Fig. 2(a) was taken at a fixed value of the Fermi level by keeping the sample in darkness during each sweep of magnetic field and illuminating it only between the successive sweeps. In this experiment, quasiparticles with a parabolic band dispersion $E(k) = \pm(\hbar k)^2/(2m)$ would produce a single dip at either positive (for holes) or negative (for electrons) magnetic field $B_c = m\omega/e$. In sample #1 the initial Fermi level lies in the valence band and the transmission demonstrates two absorption resonances in positive fields, corresponding to two sorts of quasiparticles (hole subbands). As the Fermi level is shifted to the top of the valence band, the amplitude of both resonances decreases and the low-field resonance $h_1$ approaches zero field. After 150 s of total illumination resonance $h_1$ reaches its minimal amplitude and passes through $B = 0$, while resonance $h_2$ almost vanishes at this point. The study of the universal transparency at different frequencies [Fig. 1(e)] was conducted at this position of the Fermi level. With further illumination the resonance at $B = 0$ increases and shifts to the region $B < 0$,

corresponding to negative quasiparticles. Figure 2(b) shows the value of $\sigma'_{xx}$, corresponding to the maximal absorption in resonances $h_1$-$e$. Remarkably, absorption saturates at the universal value of $\pi\alpha/2$ around the charge neutrality point. Outside this region the conductivity changes linearly with illumination up to 320 s. Further illumination does not affect the Fermi level because defects serving as charge sources become depleted.

The most probable explanation of $e$-$h$ asymmetry in the data in Fig. 2(a) is a much stronger spin splitting in the valence band in comparison to the conduction band. Evidence of such difference was demonstrated in SdH transport experiments in a tilted magnetic field, supported by theoretical calculations using the tight-binding method [33]. Following this interpretation, we attribute hole resonances $h_1$ and $h_2$ to spin-resolved cyclotron resonance (CR) in the valence band, whereas in the conduction band it appears as the single peak due to the smaller splitting. Analysis of temperature-dependent SdH oscillations in a 6.0 nm HgTe well [42] provided estimates for the masses of spin-split subbands $m_1/m_0 = 0.015$ and $m_2/m_0 = 0.03$ that are very close to the directly measured cyclotron masses, shown in Fig. 2(c). In our experiment the cyclotron massed are determined from position of the resonances as $m_c = qB_c/\omega$. Around the Dirac point (100–190 s illumination) the interband absorption peak in zero field overlaps with the intraband Drude peaks for electrons and holes $h_1$, therefore the semiclassical definition of $m_c$ loses its sense as it passes through zero. We note that we were unable to find convincing spectroscopic evidence of heavy-hole pockets [25,32,33,42–44] with $m_c/m_0 \sim 0.2$ in the samples of critical thickness. Due to the much greater expected mass the corresponding CR peak strongly broadens and becomes hard to detect at low densities.

Effects of a particle-hole asymmetry of bulk states on properties of helical edge states were recently analyzed theoretically [19–23]. A bulk asymmetry can distort the dispersion of the edge states, which is linear in the symmetric case, and shift their charge neutrality point away from the middle of the bulk gap in nearly critical wells [21,45]. Particle-hole asymmetry allows electron transitions between the edge and bulk states [19,23]. Under incident light the transitions cause spin-polarized DC current in edge channels. Thus the asymmetry facilitates generation and optical control of spin currents using CdHgTe quantum wells.

## V. CONCLUSION

Among 2D materials with a quasirelativistic spectrum HgTe wells stand out due to development of MBE growth that made them available in the form of large high-quality wafers, suitable for both technological applications and fundamental research. The large size allows comprehensive study of complex emergent phenomena by combining low-energy spectroscopy, transport, capacitance, thermodynamic, and other techniques *in situ* on the same sample. The observation of absorption determined by the fine-structure constant in coin-sized samples represents a phenomenon that is consistent with expectations for a Dirac spectrum. The precise knowledge of fine asymmetry is important for interpretation of any phenomena involving electronic properties near the charge neutrality point. The CR technique that we used can be universally applied to 2D materials to determine fine details of their band structure.

## ACKNOWLEDGMENT

This work was supported by the Austrian Science Funds (W 1243, I 3456-N27, I 5539-N).

[1] H. Ren, F. Pientka, S. Hart, A. Pierce, M. Kosowsky, L. Lunczer, R. Schlereth, B. Scharf, E. Hankiewicz, L. Molenkamp, B. Halperin, and A. Yacoby, Topological superconductivity in a phase-controlled Josephson junction, Nature (London) **569**, 93 (2019).

[2] V. L. Müller, Y. Yan, O. Kashuba, B. Trauzettel, M. Abdelghany, J. Kleinlein, W. Beugeling, H. Buhmann, and L. W. Molenkamp, Electron–hole scattering limited transport of Dirac fermions in a topological insulator, Nano Lett. **21**, 5195 (2021).

[3] D. M. Mahler, J.-B. Mayer, P. Leubner, L. Lunczer, D. Di Sante, G. Sangiovanni, R. Thomale, E. M. Hankiewicz, H. Buhmann, C. Gould, and L. W. Molenkamp, Interplay of Dirac Nodes and Volkov-Pankratov Surface States in Compressively Strained HgTe, Phys. Rev. X **9**, 031034 (2019).

[4] S. Shamim, W. Beugeling, P. Shekhar, K. Bendias, L. Lunczer, J. Kleinlein, H. Buhmann, and L. Molenkamp, Quantized spin Hall conductance in a magnetically doped two dimensional topological insulator, Nat. Commun. **12**, 3193 (2021).

[5] J. Strunz, J. Wiedenmann, C. Fleckenstein, L. Lunczer, W. Beugeling, V. Müller, P. Shekhar, N. Ziani, S. Shamim, J. Kleinlein, H. Buhmann, B. Trauzettel, and L. Molenkamp, Interacting topological edge channels, Nat. Phys. **16**, 83 (2020).

[6] L. Wu, M. Salehi, N. Koirala, J. Moon, S. Oh, and N. P. Armitage, Quantized Faraday and Kerr rotation and axion electrodynamics of the surface states of three-dimensional topological insulators, Science **354**, 1124 (2016).

[7] V. Dziom, A. Shuvaev, A. Pimenov, G. V. Astakhov, C. Ames, K. Bendias, J. Böttcher, G. Tkachov, E. M. Hankiewicz, C. Brüne, H. Buhmann, and L. W. Molenkamp, Observation of the universal magnetoelectric effect in a 3D topological insulator, Nat. Commun. **8**, 15197 (2017).

[8] A. M. Kadykov, S. S. Krishtopenko, B. Jouault, W. Desrat, W. Knap, S. Ruffenach, C. Consejo, J. Torres, S. V. Morozov, N. N. Mikhailov, S. A. Dvoretskii, and F. Teppe, Temperature-Induced Topological Phase Transition in HgTe Quantum Wells, Phys. Rev. Lett. **120**, 086401 (2018).

[9] D. But, M. Mittendorff, C. Consejo, F. Teppe, N. Mikhailov, S. Dvoretskii, C. Faugeras, S. Winnerl, M. Helm, W. Knap, M. Potemski, and M. Orlita, Suppressed Auger scattering and tunable light emission of Landau-quantized massless Kane electrons, Nat. Photonics **13**, 783 (2019).

[10] S. U. Piatrusha, E. S. Tikhonov, Z. D. Kvon, N. N. Mikhailov, S. A. Dvoretsky, and V. S. Khrapai, Topological Protection Brought to Light by the Time-Reversal Symmetry Breaking, Phys. Rev. Lett. **123**, 056801 (2019).

[11] B. C. Park, T.-H. Kim, K. I. Sim, B. Kang, J. W. Kim, B. Cho, K.-H. Jeong, M.-H. Cho, and J. H. Kim, Terahertz single conductance quantum and topological phase transitions in topological insulator $Bi_2Se_3$ ultrathin films, Nat. Commun. **6**, 6552 (2015).

[12] N. P. Armitage, E. J. Mele, and A. Vishwanath, Weyl and Dirac semimetals in three-dimensional solids, Rev. Mod. Phys. **90**, 015001 (2018).

[13] D. N. Basov, M. M. Fogler, A. Lanzara, F. Wang, and Y. Zhang, Colloquium: Graphene spectroscopy, Rev. Mod. Phys. **86**, 959 (2014).

[14] V. Varavin, S. Dvoretskii, N. Mikhailov, V. Remesnik, I. Sabinina, Y. Sidorov, V. Shvets, M. Yakushev, and A. Latyshev, Molecular beam epitaxy of CdHgTe: Current state and horizons, Optoelectron. Instrum. Data Process. **56**, 456 (2020).

[15] A. Shuvaev, V. Dziom, Z. D. Kvon, N. N. Mikhailov, and A. Pimenov, Universal Faraday Rotation in HgTe Wells with Critical Thickness, Phys. Rev. Lett. **117**, 117401 (2016).

[16] V. Dziom, A. Shuvaev, A. V. Shchepetilnikov, D. MacFarland, G. Strasser, and A. Pimenov, High-frequency breakdown of the integer quantum Hall effect in GaAs/AlGaAs heterojunctions, Phys. Rev. B **99**, 045305 (2019).

[17] K. N. Okada, Y. Takahashi, M. Mogi, R. Yoshimi, A. Tsukazaki, K. S. Takahashi, N. Ogawa, M. Kawasaki, and Y. Tokura, Observation of topological Faraday and Kerr rotations in quantum anomalous Hall state by terahertz magneto-optics, Nat. Commun. **7**, 12245 (2016).

[18] A. McRae, V. Tayari, J. Porter, and A. Champagne, Giant electron-hole transport asymmetry in ultra-short quantum transistors, Nat. Commun. **8**, 15491 (2017).

[19] V. Kaladzhyan, P. P. Aseev, and S. N. Artemenko, Photogalvanic effect in the HgTe/CdTe topological insulator due to edge-bulk optical transitions, Phys. Rev. B **92**, 155424 (2015).

[20] M. M. Mahmoodian, L. I. Magarill, and M. V. Entin, Edge absorption and pure spin current in a 2D topological insulator in the Volkov–Pankratov model, J. Phys.: Condens. Matter **29**, 435303 (2017).

[21] M. V. Durnev and S. A. Tarasenko, High-frequency nonlinear transport and photogalvanic effects in 2D topological insulators, Ann. Phys. (Berlin) **531**, 1800418 (2019).

[22] M. V. Durnev and S. A. Tarasenko, Optical properties of helical edge channels in zinc-blende-type topological insulators: Selection rules, circular and linear dichroism, circular and linear photocurrents, J. Phys.: Condens. Matter **31**, 035301 (2019).

[23] M. V. Durnev and S. A. Tarasenko, Edge photogalvanic effect caused by optical alignment of carrier momenta in two-dimensional Dirac materials, Phys. Rev. B **103**, 165411 (2021).

[24] B. A. Bernevig, T. L. Hughes, and S.-C. Zhang, Quantum spin Hall effect and topological phase transition in HgTe quantum wells, Science **314**, 1757 (2006).

[25] B. Büttner, C. X. Liu, G. Tkachov, E. G. Novik, C. Brüne, H. Buhmann, E. M. Hankiewicz, P. Recher, B. Trauzettel, S. C. Zhang, and L. W. Molenkamp, Single valley Dirac fermions in zero-gap HgTe quantum wells, Nat. Phys. **7**, 418 (2011).

[26] Z. D. Kvon, S. N. Danilov, D. A. Kozlov, C. Zoth, N. N. Mikhailov, S. A. Dvoretskii, and S. D. Ganichev, Cyclotron resonance of Dirac fermions in HgTe quantum wells, JETP Lett. **94**, 816 (2012).

[27] R. R. Nair, P. Blake, A. N. Grigorenko, K. S. Novoselov, T. J. Booth, T. Stauber, N. M. R. Peres, and A. K. Geim, Fine structure constant defines visual transparency of graphene, Science **320**, 1308 (2008).

[28] K. F. Mak, L. Ju, F. Wang, and T. F. Heinz, Optical spectroscopy of graphene: From the far infrared to the ultraviolet, Solid State Commun. **152**, 1341 (2012).

[29] S. A. Tarasenko, M. V. Durnev, M. O. Nestoklon, E. L. Ivchenko, J.-W. Luo, and A. Zunger, Split Dirac cones in HgTe/CdTe quantum wells due to symmetry-enforced level anticrossing at interfaces, Phys. Rev. B **91**, 081302(R) (2015).

[30] C. Liu, T. L. Hughes, X.-L. Qi, K. Wang, and S.-C. Zhang, Quantum Spin Hall Effect in Inverted Type-II Semiconductors, Phys. Rev. Lett. **100**, 236601 (2008).

[31] M. Orlita, K. Masztalerz, C. Faugeras, M. Potemski, E. G. Novik, C. Brüne, H. Buhmann, and L. W. Molenkamp, Fine structure of zero-mode Landau levels in $HgTe/Hg_xCd_{1-x}Te$ quantum wells, Phys. Rev. B **83**, 115307 (2011).

[32] G. M. Minkov, A. V. Germanenko, O. E. Rut, A. A. Sherstobitov, S. A. Dvoretski, and N. N. Mikhailov, Hole transport and valence-band dispersion law in a HgTe quantum well with a normal energy spectrum, Phys. Rev. B **89**, 165311 (2014).

[33] G. M. Minkov, A. V. Germanenko, O. E. Rut, A. A. Sherstobitov, M. O. Nestoklon, S. A. Dvoretski, and N. N. Mikhailov, Spin-orbit splitting of valence and conduction bands in HgTe quantum wells near the Dirac point, Phys. Rev. B **93**, 155304 (2016).

[34] Z. D. Kvon, E. B. Olshanetsky, N. N. Mikhailov, and D. A. Kozlov, Two-dimensional electron systems in HgTe quantum wells, Low Temp. Phys. **35**, 6 (2009).

[35] D. A. Kozlov, Z. D. Kvon, N. N. Mikhailov, and S. A. Dvoretsky, Weak localization of Dirac fermions in HgTe quantum wells, JETP Lett. **96**, 730 (2013).

[36] A. A. Dobretsova, Z. D. Kvon, L. S. Braginskii, M. V. Entin, and N. N. Mikhailov, Mobility of Dirac electrons in HgTe quantum wells, JETP Lett. **104**, 388 (2016).

[37] A. V. Ikonnikov, M. S. Zholudev, K. E. Spirin, A. A. Lastovkin, K. V. Maremyanin, V. Y. Aleshkin, V. I. Gavrilenko, O. Drachenko, M. Helm, J. Wosnitza, M. Goiran, N. N. Mikhailov, S. A. Dvoretskii, F. Teppe, N. Diakonova, C. Consejo, B. Chenaud, and W. Knap, Cyclotron resonance and interband optical transitions in HgTe/CdTe (013) quantum well heterostructures, Semicond. Sci. Technol. **26**, 125011 (2011).

[38] P. Olbrich, C. Zoth, P. Vierling, K.-M. Dantscher, G. V. Budkin, S. A. Tarasenko, V. V. Bel'kov, D. A. Kozlov, Z. D. Kvon, N. N. Mikhailov, S. A. Dvoretsky, and S. D. Ganichev, Giant photocurrents in a Dirac fermion system at cyclotron resonance, Phys. Rev. B **87**, 235439 (2013).

[39] V. Dziom, A. Shuvaev, N. N. Mikhailov, and A. Pimenov, Terahertz properties of Dirac fermions in HgTe films with optical doping, 2D Mater. **4**, 024005 (2017).

[40] D. J. Merthe and V. V. Kresin, Transparency of graphene and other direct-gap two-dimensional materials, Phys. Rev. B **94**, 205439 (2016).

[41] K. F. Mak, M. Y. Sfeir, Y. Wu, C. H. Lui, J. A. Misewich, and T. F. Heinz, Measurement of the Optical Conductivity of Graphene, Phys. Rev. Lett. **101**, 196405 (2008).

[42] A. Y. Kuntsevich, G. M. Minkov, A. A. Sherstobitov, Y. V. Tupikov, N. N. Mikhailov, and S. A. Dvoretsky, Density of

states measurements for the heavy subband of holes in HgTe quantum wells, Phys. Rev. B **101**, 085301 (2020).

[43] S. Hubmann, G. Budkin, M. Urban, V. Bel'kov, A. Dmitriev, J. Ziegler, D. Kozlov, N. Mikhailov, S. Dvoretsky, Z. Kvon, D. Weiss, and S. Ganichev, Impact ionization induced by terahertz radiation in HgTe quantum wells of critical thickness, J. Infrared, Millimeter, Terahertz Waves **41**, 1155 (2020).

[44] J. Gospodarič, V. Dziom, A. Shuvaev, A. A. Dobretsova, N. N. Mikhailov, Z. D. Kvon, E. G. Novik, and A. Pimenov, Band structure of a HgTe-based three-dimensional topological insulator, Phys. Rev. B **102**, 115113 (2020).

[45] M. V. Entin, M. M. Mahmoodian, and L. I. Magarill, Linearity of the edge states energy spectrum in the 2D topological insulator, Europhys. Lett. **118**, 57002 (2017).